Article

Impact of D1-V185 on the Water Molecules that facilitate O2 Formation by the Catalytic Mn4CaO5 Cluster in Photosystem II

Christopher J Kim, Han Bao, Robert L. Burnap, and Richard J. Debus

Biochemistry, **Just Accepted Manuscript** • DOI: 10.1021/acs.biochem.8b00630 • Publication Date (Web): 26 Jun 2018

Impact of D1-V185 on the Water Molecules that facilitate O_2 Formation by the Catalytic Mn_4CaO_5 Cluster in Photosystem II

Christopher J. Kim[‡], Han Bao[§,⊥], Robert L. Burnap[§], and Richard J. Debus[‡,]*

[‡]Department of Biochemistry, University of California, Riverside CA 92521,

[§]Department of Microbiology and Molecular Genetics, Oklahoma State University, Stillwater, OK 74078

Abstract

The oxidations of the O_2-evolving Mn_4CaO_5 cluster in Photosystem II are coupled to the release of protons to the thylakoid lumen via one or more proton egress pathways. These pathways are comprised of extensive networks of hydrogen-bonded water molecules and amino acid side chains. The hydrophobic residue, D1-V185, is adjacent to numerous water molecules in one of these networks. The D1-V185N mutation dramatically slows O-O bond formation. This impairment has been attributed to a disruption of the hydrogen bonded water molecules that are crucial for proton egress or whose rearrangement is required for catalysis. In this study, FTIR spectroscopy was employed to characterize the impact of the D1-V185N mutation on the carboxylate groups and water molecules that form a network of hydrogen bonds in this putative proton egress pathway. By analyzing carboxylate stretching modes, carbonyl stretching modes

of hydrogen-bonded carboxylic acids, O–H stretching modes of hydrogen-bonded water molecules, and D−O−D bending modes, we obtain evidence that the D1-V185N mutation perturbs the extensive network of hydrogen bonds that extends from Y_Z to D1-D61 to a greater extent than any mutation yet examined, but does not alter the water molecules that interact directly with D1-D61. The mutation also alters the environments of the carboxylate groups whose pK_a values change in response to the S_1 to S_2 and S_2 to S_3 transitions. Finally, the mutation alters the environment of the water molecule whose bending mode vanishes during the S_2 to S_3 transition, consistent with assigning the Ca^{2+}-bound W3 as the water molecule that deprotonates and joins oxo bridge O5 during the S_2 to S_3 transition, possibly as the second substrate water molecule for O_2 formation.

Nearly all the molecular oxygen in the biosphere is produced by the catalytic Mn_4CaO_5 cluster in Photosystem II (PSII). Molecular oxygen is released as the by-product of oxidizing water to provide the electrons and protons needed by plants, algae, and cyanobacteria to drive ATP formation and CO_2 fixation. Our understanding of water oxidation by the Mn_4CaO_5 cluster has advanced rapidly in the last five years because of new developments in X-ray crystallography and the synergism between recent structural, computational, and advanced biophysical studies (for review, see refs *1-7*). PSII is a large protein complex that is integral to the thylakoid membrane. The structure of PII has been determined to 1.85 – 1.95 Å in cyanobacteria (*8-10*), 2.78 Å in a red alga (*11*), 2.7Å in pea (*12, 13*), 3.2 Å in spinach (*14*), and 5.2 Å in *Arabidopsis thaliana* (*15*). PSII is dimeric *in vivo*, with each monomer containing 20 – 22 subunits and having a molecular weight of approximately 350 kDa. At the core of each monomer is a heterodimer of two subunits known as D1 and D2. Light-induced separations of charge within the D1/D2 heterodimer drive the oxidation of the Mn_4CaO_5 cluster, with tyrosine Y_Z serving to transfer electrons from the Mn_4CaO_5 cluster to $P_{680}^{\bullet+}$. Four electrons are removed from the Mn_4CaO_5 cluster during each catalytic cycle, advancing the cluster through five oxidation states. These states are termed S_n, where "n" denotes the number of oxidizing equivalents stored (n = 0 – 4). The S_1 state predominates in dark-adapted samples. The S_4 state is a transient intermediate whose formation triggers the utilization of the four stored oxidizing equivalents to form O_2 from two substrate-water-derived metal ligands, the regeneration of the S_0 state, and the binding of at least one of two new substrate water molecules. The cluster's metal ions are ligated by six carboxylate groups, one histidine side chain, and four water molecules. All but one of the amino acid ligands are provided by the D1 subunit.

In the highest resolution structures, the Mn_4CaO_5 cluster consists of a distorted Mn_3CaO_4 cube that is linked to a fourth Mn ion (denoted Mn4) by two oxo bridges (denoted O4 and O5, see Figure 1). Considerable evidence supports identifying O5 as the deprotonated form of one of the two substrate water molecules (*16-19*). It is present as a μ-hydroxo bridge in the S_0 state (*19*) and as a fully deprotonated μ-oxo bridge in the S_2 state (*16*). The Mn_4CaO_5 cluster is structurally flexible. In the S_2 state it interconverts between two nearly isoenergetic conformations (*20*). In one conformation, O5 coordinates to Mn4, leaving Mn1 five-coordinate. In the second conformation, O5 coordinates to Mn1, leaving Mn4 five-coordinate. During the S_2 to S_3 transition, an additional oxygen joins O5 between Mn4 and Mn1 (*21-25*). This additional oxygen [denoted O6 (*25*)] has been proposed to correspond to a water molecule that deprotonates and relocates from the Mn4-bound W2 position (*26-32*) or the Ca^{2+}-bound W3 position (*33-38*). It is thought to correspond to a deprotonated form of the second substrate water molecule (*22, 23, 25, 27, 29-31, 33-37, 39-42*). Its relocation to a position between Mn4 and Mn1 and adjacent to O5 during the S_2 to S_3 transition would ensure that the two substrate oxygen atoms have opposite spins as the O-O bond is formed in the S_4 state, substantially decreasing the activation energy for bond formation (*22, 23, 39, 43*). The relocation also would ensure that the two oxygen atoms that will form the O-O bond are held in close proximity only after the S_3 state is fully formed, thereby preventing deleterious catalase-like activity in the lower S states (*23, 41*). The subsequent formation of the $Y_Z^{\bullet}S_3$ state locks the two oxygen atoms in position for O-O bond formation in the S_4 state (*44*).

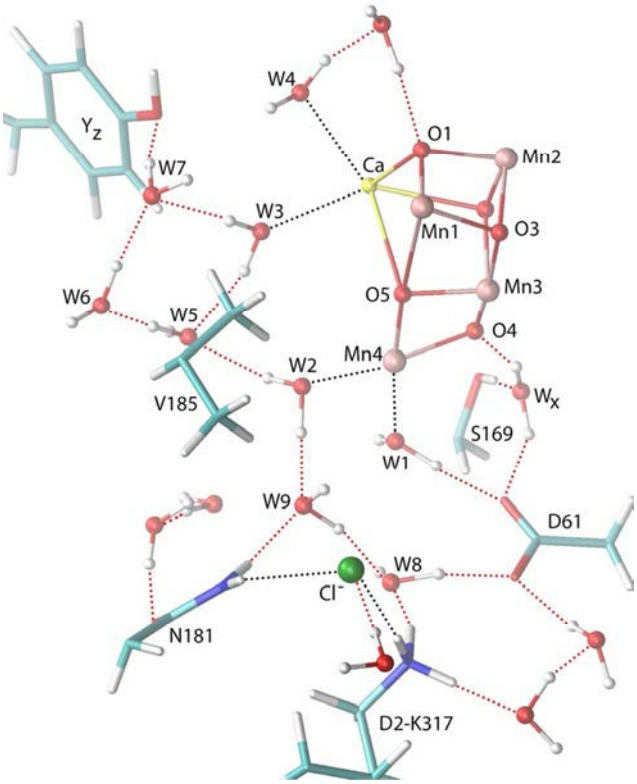

FIGURE 1. Water molecules and selected residues in the vicinity of the Mn_4CaO_5 cluster. Residues are from the D1 subunit unless noted otherwise. Salmon-colored spheres, manganese ions; yellow sphere, calcium; green sphere, chloride; red spheres, oxygen atoms of μ-oxo bridges and water molecules. The coordinates for this figure were constructed with QM/MM methods (*45*) based on the coordinates in the 1.9 Å X-ray crystallographic model (*8*) and were kindly provided by V. S. Batista and coworkers.

The oxidations of the Mn_4CaO_5 cluster are coupled to the release of protons, with electrons and protons being removed alternatively as the S state cycle proceeds (*46-48*). The alternating deprotonations and oxidations prevent the redox potential of the Mn_4CaO_5 cluster from rising to levels that prevent its subsequent oxidation by the $Y_Z^{\bullet}$ radical anion. Deprotonation of the Mn_4CaO_5 cluster takes place via one or more proton egress pathways that

link the Mn_4CaO_5 with the thylakoid lumen. These pathways are comprised of networks of hydrogen-bonded water molecules and protonatable amino acid side chains [e.g., refs *49-57*]. Elements of these networks are undoubtedly dynamic in nature (*51, 58*). One such network includes a series of hydrogen-bonded water molecules that stretches from Y_Z to D1-D61 (see Figure 1). D1-D61 is the initial residue of a proton egress pathway that facilitates the S_3 to S_4 transition (*59-65*). Adjacent to numerous water molecules in this network is the hydrophobic residue, D1-V185. The side-chain of this residue lies 3.7 Å from O5 and 3-5 Å from waters W2, W3, W5, W6, and W7. The D1-V185N mutation has been shown to dramatically slow the rate of O_2 release and extend the kinetic lag phase of the S_3 to S_4 transition (*66*). This lag phase occurs prior to Mn reduction/O_2 formation has been attributed to proton movement (*46-48, 67, 68*) and/or a structural rearrangement (*69*). The alterations caused by the D1-V185N mutation have been attributed to a disruption of the hydrogen bonded water molecules in the proton egress pathway that facilitates the S_3 to S_4 transition (*66*). Indeed, the D1-V185N mutation was constructed to disrupt the orientation and dynamics of these water molecules (*66*).

FTIR difference spectroscopy is an ideal method for characterizing structural changes (*70-73*) and has been employed extensively to study the S state cycle in PSII (*74-80*). FTIR is especially suited for probing changes in hydrogen bonding. In PSII, the C=O stretching modes of hydrogen-bonded carboxylic acids have been monitored in the 1760 – 1730 cm^{-1} region (*63, 65, 81-85*), the N-H stretching mode of a protonated histidyl group has been monitored in the 3000 – 2400 cm^{-1} region (*86*), the O–H stretching modes of weakly hydrogen-bonded water molecules have been monitored in the 3700 – 3500 cm^{-1} region (*65, 84, 85, 87-94*), the O–H stretching modes of strongly hydrogen-bonded water molecules have been monitored in the 3200 – 2500 cm^{-1} region (*65, 84, 85, 88, 93-95*), and D−O−D bending modes have been

monitored in the 1250 – 1150 cm^{-1} region (*65, 94, 96*). In this study, we employed FTIR spectroscopy to characterize the impact of the D1-V185N mutation on the carboxylate groups and water molecules that form part of a putative proton egress pathway leading from the Mn_4CaO_5 cluster to the thylakoid lumen. We find that the D1-V185N mutation perturbs this network to a greater extent than any other mutation yet examined, alters the environments of the carboxylate groups whose pK_a values change in response to the S_1 to S_2 and S_2 to S_3 transitions, and alters the environment of the water molecule whose D-O-D bending mode disappears during the S_2 to S_3 transition. The latter observation is consistent with identifying W3 as the water molecule that deprotonates and joins O5 during the S_2 to S_3 transition.

MATERIALS AND METHODS

Construction of Mutant and Propagation of Cultures. Cells and thylakoid membranes of the D1-V185N mutation-bearing strain of *Synechocystis* sp. PCC 6803 have been characterized previously (*66*). The mutation was constructed in the *psbA-2* gene of *Synechocystis* sp. PCC 6803 and transformed into a strain of *Synechocystis* that lacks all three *psbA* genes and contains a hexahistidine-tag (His-tag) fused to the C-terminus of CP47 (*97*). The wild-type strain described in this manuscript was constructed in an identical manner as the D1-V185N strain but with a transforming plasmid that carried no mutation. Large-scale cultures were propagated as described previously (*98*).

Purification of PSII core complexes. Oxygen-evolving PSII core complexes were purified as described previously in buffer containing 1.2 M betaine, 10% (v/v) glycerol, 50 mM MES-NaOH (pH 6.0), 20 mM $CaCl_2$, 5 mM $MgCl_2$, 50 mM histidine, 1 mM EDTA, and 0.03% (w/v) *n*-dodecyl *β*-D-maltoside (*65*). These were concentrated to approx. 1 mg of Chl/mL, flash-

frozen, and stored at −80 °C.

Preparation of FTIR samples. PSII core complexes were transferred into 40 mM sucrose, 10 mM MES-NaOH (pH 6.0), 5 mM $CaCl_2$, 5 mM NaCl, 0.06% (w/v) *n*-dodecyl β-D-maltoside, concentrated, mixed with 1/10 volume of fresh 100 mM potassium ferricyanide, then dried lightly with dry N_2 gas (*94*). Samples were then rehydrated and maintained at a relative humidity of 95% by spotting six 1 μL droplets of 40% (v/v) glycerol in water around the window's periphery before a second window was placed on the first with a thin o-ring spacer in between. For samples having natural abundance $H_2{}^{16}O$ exchanged for $D_2{}^{16}O$ or $D_2{}^{18}O$, the lightly dried samples were rehydrated with 40% (v/v) glycerol$(OD)_3$ (98% D, Cambridge Isotope Laboratories, Inc., Andover, MA) in $D_2{}^{16}O$ (99.9% D, Cambridge Isotope Laboratories, Inc., Andover, MA) or $D_2{}^{18}O$ (98% D, 97% 18O, Cambridge Isotope Laboratories, Inc., Andover, MA), respectively (*65, 94, 96*). Sealed samples were equilibrated in the FTIR sample compartment at 0°C in darkness for 1.5 h, illuminated with 6 pre-flashes, then dark-adapted for 30 min (*65, 94*). For each sample, the absorbance at 1657 cm^{-1} (amide I band) was 0.6 – 1.1.

FTIR Spectroscopy. Spectra were recorded with a Bruker Vertex 70 spectrometer (Bruker Optics, Billerica, MA) outfitted with a pre-amplified, midrange D317 photovoltaic MCT detector (Kolmar Technologies, Inc., Newburyport, MA), as described in ref. (*94*). After dark adaptation, samples were given six flashes at 13 s intervals. Two transmission spectra were recorded before the first flash and one transmission spectrum was recorded starting 0.33 s after the first and subsequent flashes (each transmission spectrum consisted of 100 scans). The 0.33 s delay was included to allow the oxidation of $Q_A^{\bullet-}$ by the ferricyanide. Difference spectra of the successive S-state transitions (e.g., S_{n+1}–*minus*–S_n difference spectra, henceforth written $S_{n+1}-S_n$), were obtained by dividing the transmission spectrum obtained after the n^{th} flash by the

transmission spectrum obtained before the n^{th} flash, then converting the ratio to units of absorption. The background noise level and the stability of the baseline were obtained by dividing the second pre-flash transmission spectrum by the first and converting the ratio to units of absorption (these spectra are labeled dark−dark in each figure – these are control difference spectra obtained *without* a flash being given). The sample was then dark-adapted for 30 min and the cycle was repeated. For each sample, the illumination cycle was repeated 15 times. The spectra of 20-61 samples were averaged (see figure legends). The amplitudes of the D1-V185N difference spectra were multiplied by factors of 1.2 to 2.4 to normalize the peaks corresponding to the reduction of ferricyanide to ferrocyanide by $Q_A^{\bullet-}$ (at 2115 and 2037 cm^{-1}, respectively) to those in the corresponding wild-type spectra (this procedure normalizes the spectra to the extent of flash-induced charge-separation).

Other Procedures. Chlorophyll concentrations were determined as described in ref. (*99*).

RESULTS

Midfrequency Region. The mid-frequency difference spectra produced by four flashes given to wild-type and D1-V185N PSII core complexes are compared in Figure 2 (black and red traces, respectively). The spectra produced by the first, second, third, and fourth flashes of the wild-type samples closely resemble spectra presented previously for PSII preparations from *Synechocystis* sp. PCC 6803, *Thermosynechococcus elongatus*, and spinach, and correspond predominantly to S_2-S_1, S_3-S_2, S_0-S_3, and S_1-S_0 difference spectra, respectively [e.g., refs. (*74-76, 78-80, 100-102*)]. The S_2-S_1 spectrum of D1-V185N PSII core complexes (upper red trace in Figure 2) showed substantial changes in throughout the mid-frequency region. In the amide I region, the 1707(-) cm^{-1} feature was enhanced and a positive feature appeared at 1677 cm^{-1} in

place of the 1681(-) cm^{-1} and 1672(+) cm^{-1} features of the wild-type. In the asymmetric carboxylate stretching [$\nu_{asym}(COO^-)$] and amide II region, the 1629(-) cm^{-1} feature was enhanced, a positive feature appeared at 1603 cm^{-1}, the 1587(+) cm^{-1}, 1560(-) cm^{-1}, and 1544(-) cm^{-1} features were diminished substantially, a negative feature appeared at 1573 cm^{-1}, and the 1531(+)/1523(-) cm^{-1} derivative feature was eliminated. The features in the symmetric carboxylate stretching [$\nu_{sym}(COO^-)$] region were diminished: the 1416(-)/1410 (+) cm^{-1} derivative feature shifted to 1423(-)/1416(+) cm^{-1}, the 1400 (-) cm^{-1} feature shifted to 1388(-) cm^{-1}, the 1364(+) cm^{-1} and 1354(-) cm^{-1} features shifted to 1368(+) cm^{-1} and 1360(-) cm^{-1}, respectively, and a small positive feature appeared at 1288 cm^{-1}. Also, the 1260(+)/1250(-) cm^{-1} feature was diminished. In the carbonyl stretching [ν(C=O)] region, the 1746(-) cm^{-1} feature was diminished and replaced by a negative feature at 1737 cm^{-1}. An expanded view of this region is shown in Figure 3 (top left panel).

The S_3-S_2 spectrum of D1-V185N also showed changes throughout the mid-frequency region (second set of traces in Figure 2). In the amide I region, a negative feature appeared at 1704 cm^{-1}, the 1697(+) cm^{-1} feature was enhanced, the 1687(-) cm^{-1} and 1675(-) cm^{-1} features were diminished, and the 1675(-)/1666(+)/1659(-) cm^{-1} feature was replaced with a

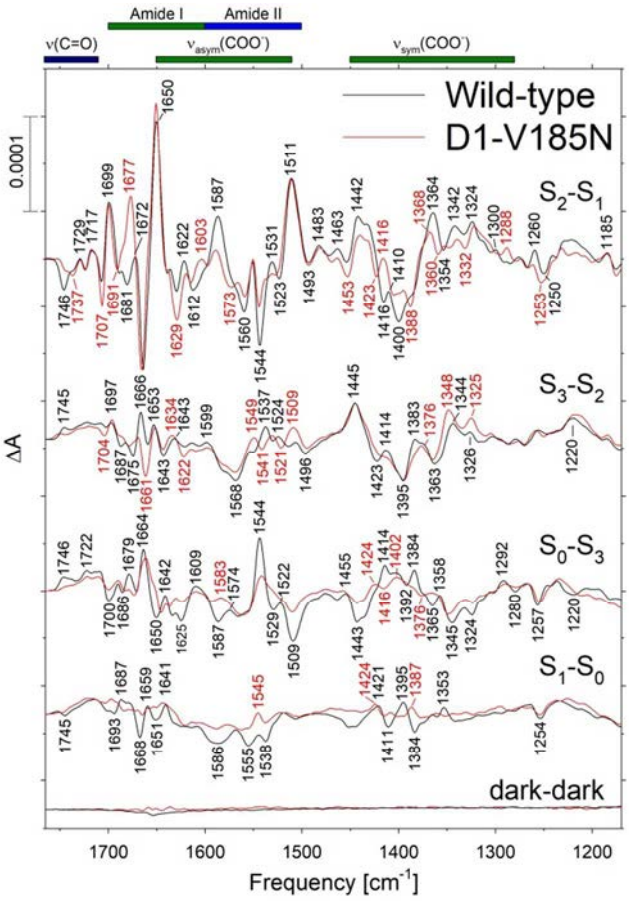

FIGURE 2. Mid-frequency FTIR difference spectra of wild-type (black) and D1-V185N (red) PSII core complexes in response to four successive flash illuminations applied at 0ºC. The data (plotted from 1770 cm^{-1} to 1170 cm^{-1}) represent the averages of 22 wild-type and 20 D1-V185N samples (33,000 and 30,000 scans, respectively). The D1-V185N spectra were multiplied vertically by factors of 1.2 to 1.4 to approximately normalize the wild-type and mutant spectra to the extent of flash-induced charge separation. The dark-dark control trace of the mutant (lower red trace) also multiplied by a factor of 1.4. The dark-dark control traces show the noise level and the stability of the baseline.

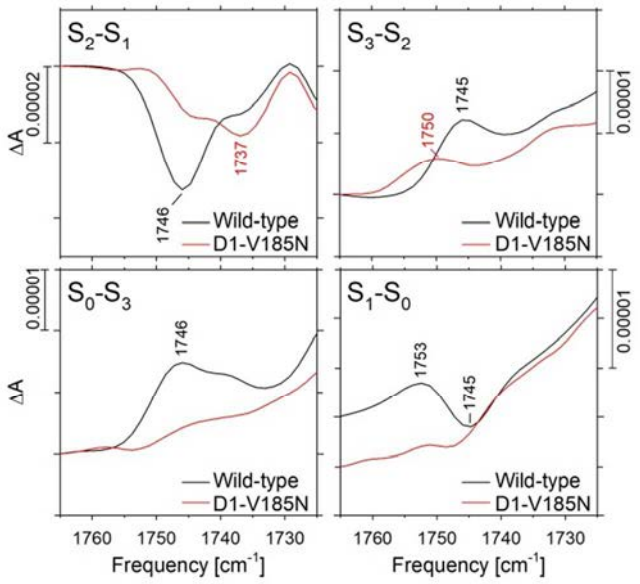

FIGURE 3. FTIR difference spectra of wild-type (black) and D1-V185N (red) PSII core complexes in the ν(C=O) region. The data are expanded from those shown in Figure 2.

negative feature at 1661 cm^{-1}. In the $\nu_{asym}(COO^-)$/amide II region, a negative feature appeared at 1622 cm^{-1}, and the 1537(+) cm^{-1} and 1524(+) cm^{-1} features were replaced with a 1549(+)/1541(-)/1531(+)/1521(-)/1509(+) cm^{-1} feature. In the $\nu_{sym}(COO^-)$ region, the 1423(-)/1414(+) cm^{-1} derivative feature was eliminated, the 1383(+) cm^{-1} feature shifted to 1376 cm^{-1}, and the 1344(+) cm^{-1} feature shifted to 1348 cm^{-1}. In the ν(C=O) region, the 1746(+) cm^{-1} feature was diminished and shifted to 1750 cm^{-1}. An expanded view of this region is shown in Figure 3 (top right panel).

The S_0-S_3 spectrum of D1-V185N was diminished substantially in amplitude and showed substantial changes throughout the mid-frequency region (Figure 2, 3rd set of traces). In the amide I region, the 1700(-) cm^{-1} and 1679(+) cm^{-1} features were nearly eliminated. In the $\nu_{asym}(COO^-)$/amide II region, the 1650(-) cm^{-1} feature shifted to 1646 cm^{-1}, the 1642(+) cm^{-1} and 1625(-) cm^{-1} features were eliminated, the 1587(-) cm^{-1} feature was replaced with a 1583(+) cm^{-1} feature, the 1544(+) cm^{-1} and 1509(-) cm^{-1} features were sharply diminished, and the 1529(-)/1522(+) cm^{-1} feature was eliminated. In the $\nu_{sym}(COO^-)$ region, the 1443(-) cm^{-1} feature was sharply diminished, and the 1414(+)/1392(-)/1384(+)/1365(-)/1358(+) cm^{-1} feature was replaced with a 1424(+)/1416(-)/1402(+)/1376(-)/1365(+) cm^{-1} feature, the 1345(-) cm^{-1} feature shifted to 1349(-) cm^{-1}, and the 1324(-) and 1280(-) cm^{-1} features were diminished. In the ν(C=O) region, the 1746(+) cm^{-1} feature was eliminated (see expanded view in Figure 3, lower left panel).

The S_1-S_0 spectrum of D1-V185N also was diminished substantially in amplitude and showed substantial changes throughout the mid-frequency region (Figure 2, 4th set of traces). In the $\nu_{sym}(COO^-)$ region, the 1421(+) cm^{-1} and 1395(+) cm^{-1} features shifted to 1424(+) cm^{-1} and 1387(-) cm^{-1}, respectively. Most other features throughout in the mid-frequency region were sharply diminished or eliminated. In the ν(C=O) region, the 1753(+)/1745 cm^{-1} derivative feature was eliminated (see expanded view in Figure 3, lower right panel).

Strongly H-bonded O–H stretching region. The O–H stretching vibrations of strongly H-bonded OH groups are observed as very broad positive features between 3200 and 2500 cm^{-1} (*65, 84, 85, 88, 93-95*). These features have been observed in PSII core complexes from *Synechocystis* sp. PCC 6803 and *Thermosynechococcus elongatus* and in PSII membranes from spinach and are diminished or eliminated (presumably downshifted) in the presence of D_2O (*65, 88*). These regions of wild-type and D1-V185N PSII core complexes are compared in Figure 4.

In the S_2-S_1 spectrum (Figure 4, upper traces), the broad feature is overlain with numerous positive features that correspond to C–H stretching vibrations from aliphatic groups and N–H stretching vibrations and their Fermi resonance overtones from the imidazole group(s) of one or more histidine residues (*87, 88, 103*). Our data show that the D1-V185N mutation causes only slight perturbations in this region of any of the difference spectra.

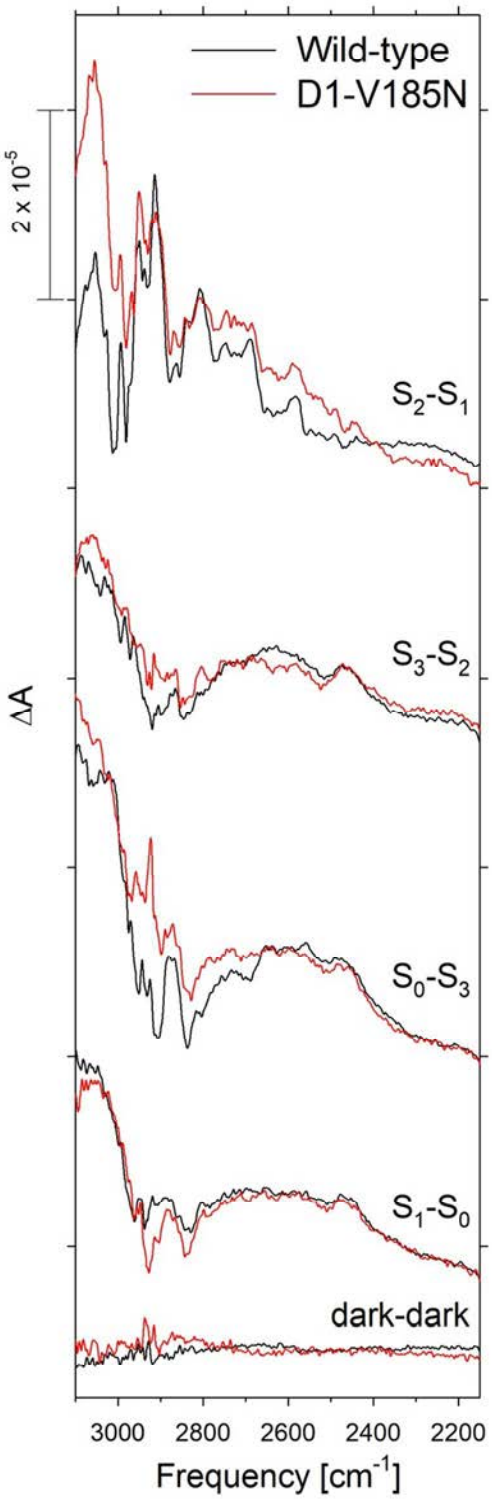

FIGURE 4. FTIR difference spectra of wild-type (black) and D1-V185N (red) PSII core complexes between 3100 and 2150 cm^{-1} in response to four successive flash illuminations applied at 0°C. The data were collected simultaneously with that shown in Figure 2. The spectra

of the D1-V185N samples were multiplied vertically as in Figure 2, and were shifted vertically to coincide approximately at 3700 cm^{-1}. Dark-dark control traces show the noise level and the stability of the baseline (lower traces).

Weakly H-bonded O–H stretching region. The O–H stretching vibrations of weakly hydrogen bonded OH groups of water molecules appear between 3700 and 3500 cm^{-1}. These features are shifted 930-960 cm^{-1} to lower frequencies in $D_2{}^{16}O$ and approximately 10 cm^{-1} to lower frequencies in $H_2{}^{18}O$ (*65, 87, 88, 104*). These features have been examined in PSII from *Thermosynechococcus elongatus* (*87-89, 96*), *Synechocystis* sp. PCC 6803 (*65, 84, 85, 90, 92, 94*), and spinach (*91, 93*). In our wild-type samples, this region of the S_2-S_1 spectrum exhibited a weak negative feature at 3663 cm^{-1}, a weak positive feature at 3617 cm^{-1}, and a large negative feature at 3584 cm^{-1} (Figure 5, upper black trace). Corresponding features in the O–D region were observed at 2710(–) cm^{-1}, 2682(+) cm^{-1}, and 2650(–) cm^{-1} (Figure 6, upper black trace). The D1-V185N mutation diminished the 3663(-) cm^{-1} feature and replaced the broad positive feature centered at 3617 cm^{-1} with a broad negative feature centered at 3619 cm^{-1} (Figure 5, upper black trace). Corresponding D1-V185N-induced changes were observed in the O–D region of the S_2-S_1 spectrum (Figure 6, upper red trace): the negative feature at 2710 cm^{-1} was diminished and the broad positive feature centered at 2682 cm^{-1} was replaced with a broad negative feature centered at 2683 cm^{-1}.

The weakly hydrogen bonded O–H regions of the S_3-S_2, S_0-S_3, and S_1-S_0 spectra in our wild-type samples showed broad negative features centered at approximately 3600, 3618, and 3611 cm^{-1}, respectively (Figure 5, lower black traces). The corresponding negative features in the O–D regions showed minima at 2634, 2675, and 2663 cm^{-1}, respectively (Figure 6, lower

black traces). The apparent D1-V185N-induced decrease in the intensity of the 3600 cm^{-1} feature in the S_3-S_2 spectrum (Figure 5, second red trace) may be the result of a shift in the baseline because similar mutation-induced decrease was not observed in the O–D region (Figure 6, second red trace). The D1-V185N mutation produced little significant change in the O–H or O–D regions of the S_0-S_3 or S_1-S_0 spectra (Figures 5 and 6, third and fourth sets of traces).

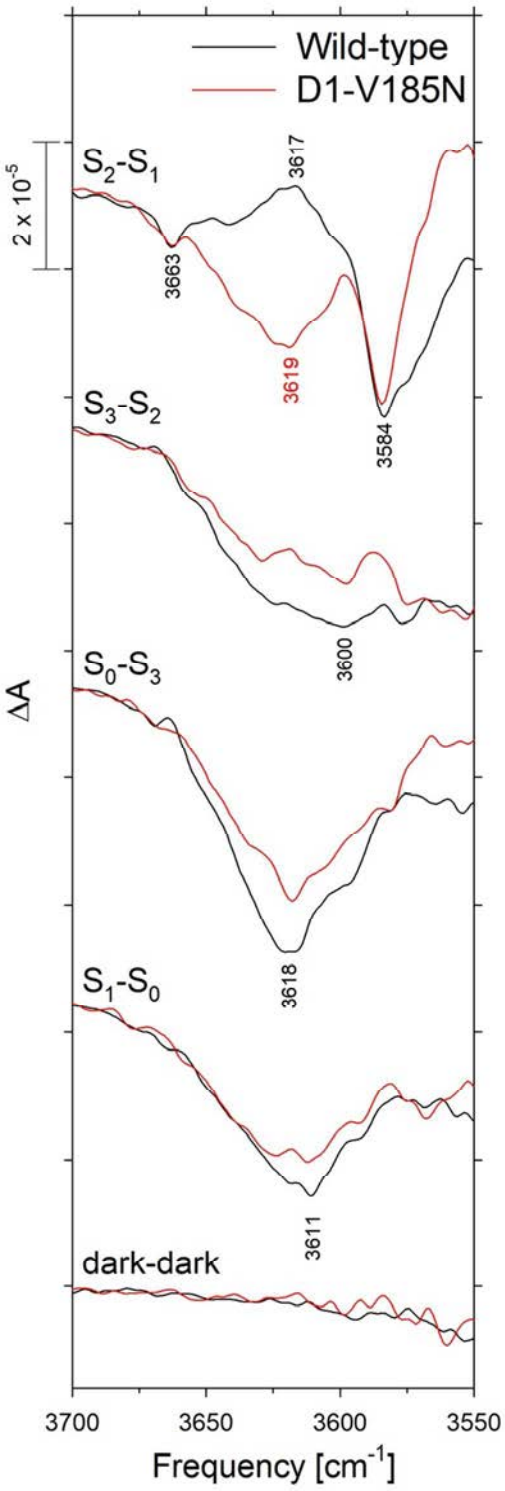

FIGURE 5. FTIR difference spectra of wild-type (black) and D1-V185N (red) PSII core complexes in the weakly hydrogen bonded O–H stretching region in response to four successive

flash illuminations applied at 0°C. The data were collected simultaneously with that shown in Figure 2, were multiplied vertically as in Figure 2, and were shifted vertically to coincide approximately at 3700 cm^{-1}. Dark-dark control traces show the noise level and the stability of the baseline (lower traces).

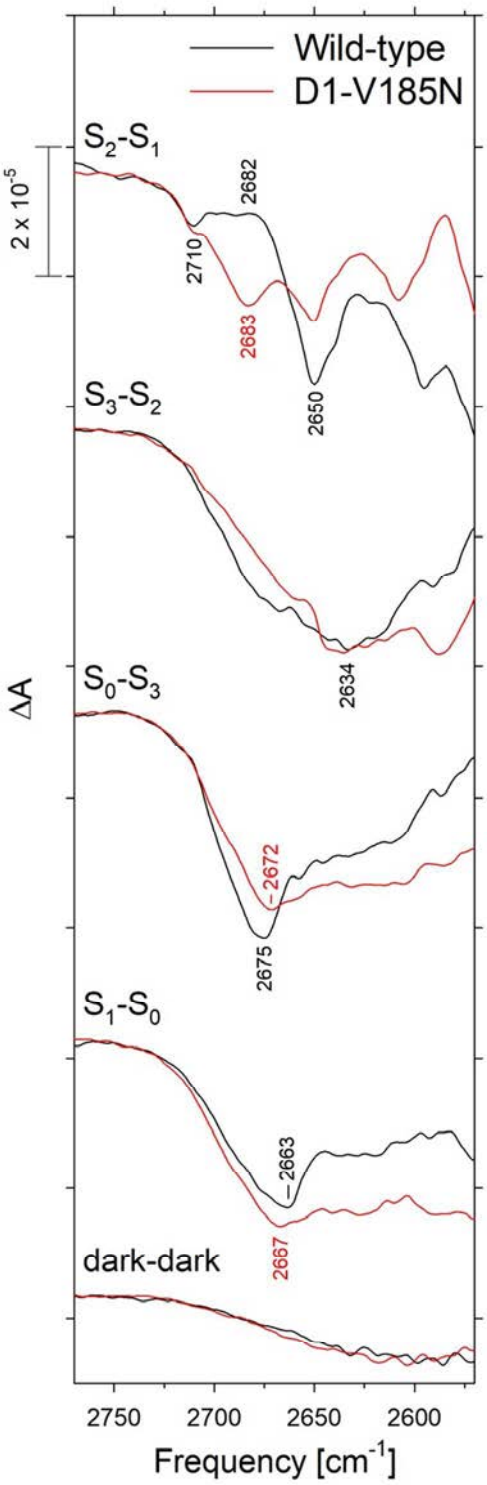

FIGURE 6. FTIR difference spectra of wild-type (black) and D1-V185N (red) PSII core complexes in the O–D stretching region in response to four successive flash illuminations

applied at 0°C. The data represent the averages of 32 wild-type and 61 D1-V185N samples (48,000 and 90,300 scans, respectively) after hydration with $D_2{}^{16}O$ and were recorded simultaneously with the $D_2{}^{16}O$ data shown in Figures 7 and 8, respectively. The D1-V185N spectra were multiplied vertically by factors of 1.2 as in Figure 8 and were shifted vertically to coincide approximately at 2750 cm^{-1}. Dark-dark control traces show the noise level and the stability of the baseline (lower traces).

D-O-D Bending Region. D-O-D vibrational modes appear near 1210 cm^{-1} (*96, 105*) and are inherently weak. However, they can be observed in $D_2{}^{16}O$-$D_2{}^{18}O$ double difference spectra (*65, 94, 96*). The mid-frequency FTIR difference spectra of wild-type PSII hydrated with $D_2{}^{16}O$ or $D_2{}^{18}O$ are shown in Figure 7. The corresponding spectra of D1-V185N are shown in Figure 8. In Figure 8, the difference spectra of the mutant samples were multiplied vertically by factors of 1.2 normalize the spectra to the amplitudes of the negative peak of ferricyanide at 2115 cm^{-1} and the positive peak of ferrocyanide at 2037 cm^{-1} in the corresponding wild-type spectra shown in Figure 7. To calculate the $D_2{}^{16}O$-$D_2{}^{18}O$ double difference spectra, the difference spectra shown in Figures 7 and 8 were subtracted directly. The resulting S_{n+1}-S_n $D_2{}^{16}O$-$D_2{}^{18}O$ double difference spectra of wild-type and D1-V185N in the D-O-D bending [δ(DOD)] region are compared in Figure 9 (black and red traces, respectively). The double difference spectra for the wild-type PSII core complexes resembled those reported previously for *Thermosynechococcus elongatus* (*96*) and *Synechocystis* sp. PCC 6803 (*65, 94*). The negative feature at 1263 cm^{-1} in the S_2-S_1 double difference spectrum was reported previously in spectra from *Thermosynechococcus elongatus* and was not assigned to a δ(DOD) mode (*96*). It has not been reported previously in spectra from *Synechocystis* sp. PCC 6803 (*65, 94*). It may be relevant that samples exhibiting

this feature were equilibrated at a relative humidity of 95% (Ref. (*96*) and this study), whereas samples not exhibiting this feature were equilibrated at a relative humidity of 99% (*65, 94*).

In the S_2-S_1 $D_2{}^{16}O$-*minus*-$D_2{}^{18}O$ double difference spectrum, the D1-V185N mutation shifted the intense 1221(-) and 1210(+) cm^{-1} to 1224(-) and 1212(+) cm^{-1}, respectively, shifted the less intense 1188(-) and 1174(+) cm^{-1} features to 1196(-) and 1184(+) cm^{-1}, respectively, and eliminated the negative feature at 1263 cm^{-1} (Figure 9, upper pair of traces). In the S_3-S_2 $D_2{}^{16}O$-$D_2{}^{18}O$ double difference spectrum, the D1-V185N mutation shifted the weak 1200(+) and 1192(-) cm^{-1} features to 1194(+) and 1184(-) cm^{-1}, respectively, diminished the 1238(-) cm^{-1} feature and shifted it to 1232 cm^{-1}, and eliminated the 1265(-) and 1171(+) cm^{-1} features. There were few recognizable features in the S_0-S_3 and S_1-S_0 $D_2{}^{16}O$-$D_2{}^{18}O$ double difference spectra (Figure 9, lower two pairs of traces), possibly because of the lower amplitudes of the S_0-S_3 and S_1-S_0 difference spectra, as was observed in spectra equilibrated with H_2O (Figure 2).

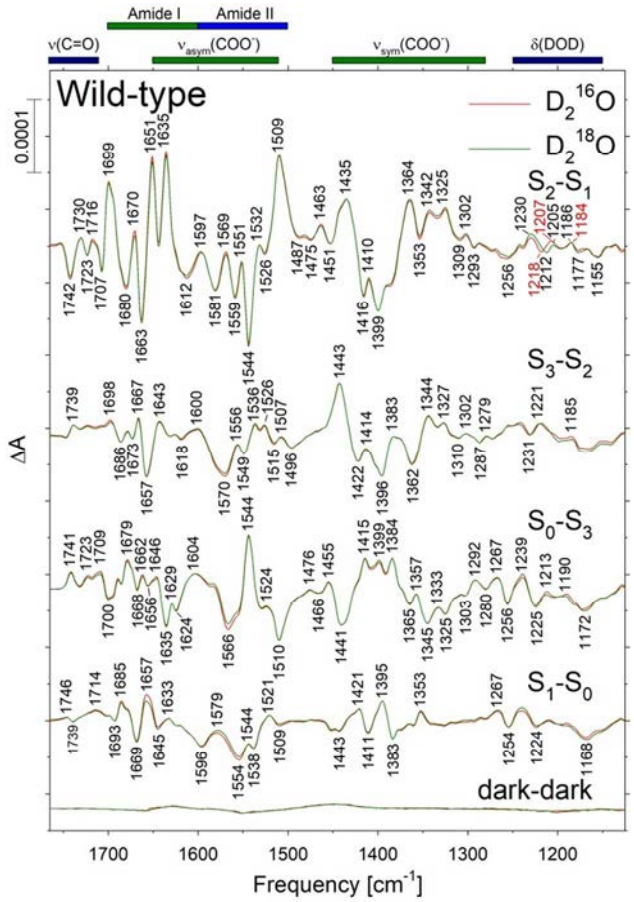

FIGURE 7. Mid-frequency FTIR difference spectra of wild-type PSII core complexes in response to four successive flash illuminations applied at 0°C after hydration with $D_2{}^{16}O$ (red) or $D_2{}^{18}O$ (green). The $D_2{}^{16}O$ and $D_2{}^{18}O$ data represent the averages of 32 samples (48,000 scans for each trace) and 30 samples (44,400 scans for each trace), respectively. The dark-dark control traces show the noise level and the stability of the baseline (lower traces).

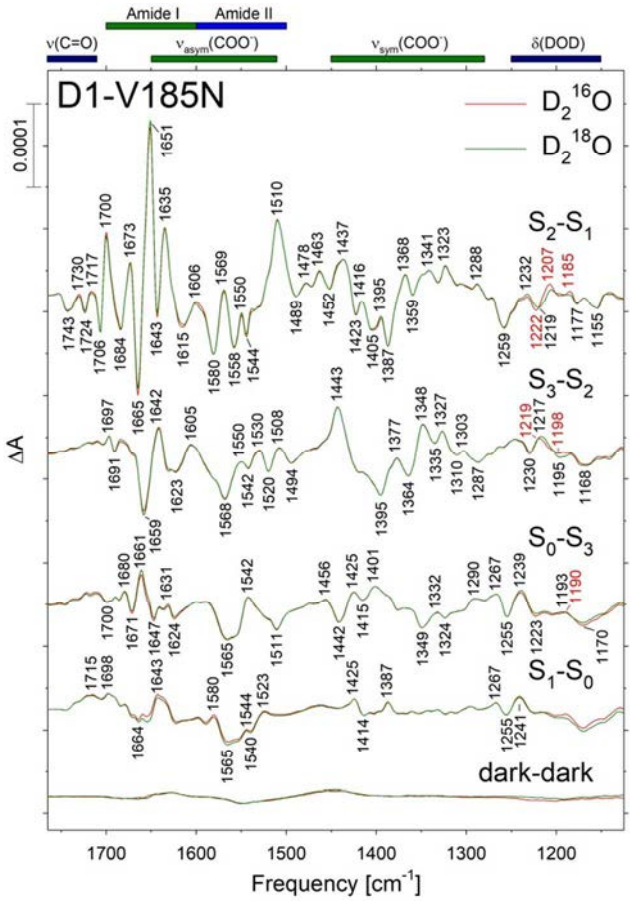

FIGURE 8. Mid-frequency FTIR difference spectra of D1-V185N PSII core complexes in response to four successive flash illuminations applied at 0°C after hydration with $D_2{}^{16}O$ (red) or $D_2{}^{18}O$ (green). The $D_2{}^{16}O$ and $D_2{}^{18}O$ data represent the averages of 61 samples (90,300 scans for each trace) and 60 samples (89,900 scans for each trace), respectively. The D1-V185N spectra have been multiplied vertically by factors of 1.2 to approximately normalize the spectra to the extent of flash-induced charge separation in the corresponding wild-type spectra of Figure 7. The dark-dark control traces were also multiplied by factors of 1.2 and show the noise level and the stability of the baseline (lower traces).

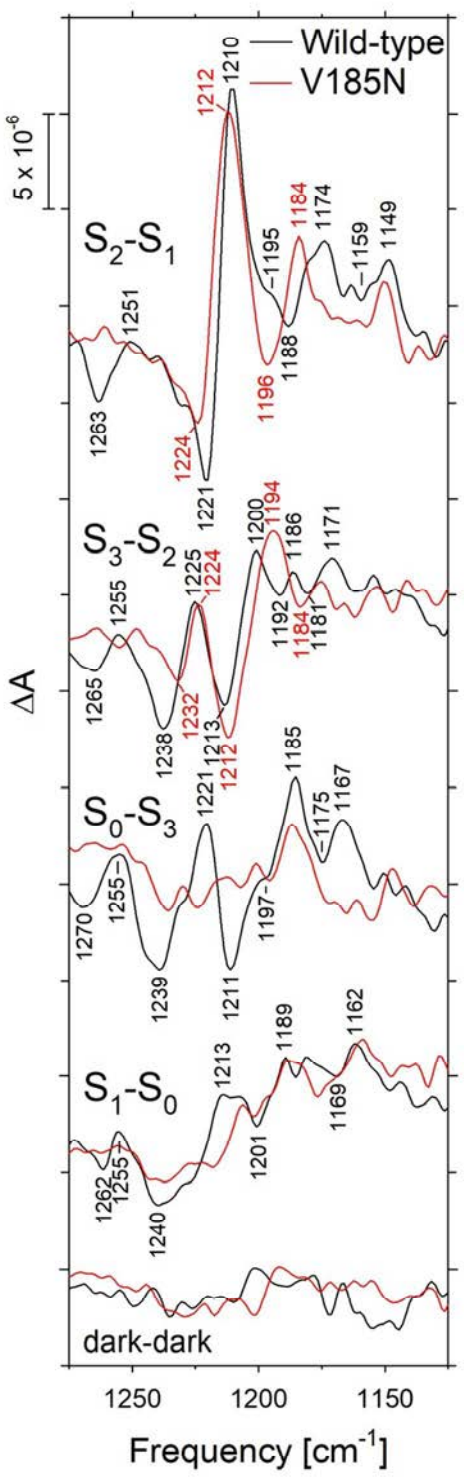

FIGURE 9. The S_{n+1}-S_n $D_2{}^{16}O$-$D_2{}^{18}O$ double difference spectra of wild-type (black) and D1-V185N (red) PSII core complexes in the D-O-D bending region. The data of Figures 7 and 8

were subtracted directly but were offset vertically to maximize overlap. The lower traces show the noise levels and were obtained by calculating the $D_2{}^{16}O$-$D_2{}^{18}O$ difference spectra of the dark-dark traces shown in Figures 7 and 8.

DISCUSSION

Carboxylate Residues. The oxidations of the Mn_4CaO_5 cluster during the S state cycle alter $\nu_{sym}(COO^-)$ and $\nu_{asym}(COO^-)$ modes of carboxylate groups and amide I and amide II modes in the polypeptide backbone (*101, 102, 106*). On the basis of a recent QM/MM study, it was concluded that multiple carboxylate ligands of the Mn_4CaO_5 cluster contribute to most of the features in the $\nu_{sym}(COO^-)$ region of the S_2-S_1 spectrum (*107*). However, the individual mutation of four of the Mn_4CaO_5 clusters carboxylate ligands, D1-D170H (*108, 109*), D1-E189Q (*110, 111*), D1-E189R (*111*), D1-E333Q (*92*), and D1-D342N (*98*) produced little or no changes to any of the mid-frequency S_{n+1}-S_n FTIR difference spectra (also see ref. (*112*)). Experimentally, mutations constructed at residues involved in the network of hydrogen bonds that extend from Y_Z to D1-D61 and the D1-E65/D1-R334/D2-E312 triad and located 5 – 11 Å from the nearest Mn ion (e.g., D1-D61A, D1-E65A, D1-N87A, D1-Q165E, D1-N181A, D1-R334A, D2-E312A, and D2-K317A), cause numerous changes throughout the mid-frequency FTIR difference spectra, including in the $\nu_{sym}(COO^-)$ region of the S_2-S_1 spectrum (*63, 65, 81, 83-85*).

Because D1-V185 is located adjacent to numerous water molecules in the network of hydrogen bonds that links Y_Z with D1-D61, the D1-V185N mutation would be expected to substantially perturb this network. Indeed, the D1-V185N mutation alters features in the $\nu_{sym}(COO^-)$ and $\nu_{asym}(COO^-)$/amide II regions of the S_2-S_1 spectrum to a greater extent than any mutation yet examined. In the $\nu_{sym}(COO^-)$ region, the substantial decrease of the 1400(-) cm^{-1}

feature is also produced by the D1-Q165E and D1-R334Q mutations (*83*). The substantial decrease of the 1364(+) cm^{-1} feature is also produced by the D1-D61A (*65*), D1-Q165E (*83*), D1-R334A (*83*), and D2-E312A (*63*) mutations, by the substitution of Sr^{2+} for Ca^{2+} (*93, 94, 113-116*), and to lesser extents by the D1-N181A (*84*) and D2-K317A (*81*) mutations. Finally, alteration of the 1416(-)/1410(+) cm^{-1} feature is also produced by D1-D61A (*65*), D1-N87A (*85*), D1-N181A (*84*), D1-R334A (*83*), and D2-K317A (*81*) mutations. In the $\nu_{asym}(COO^-)$/amide II region, the substantial decrease of the 1587(+) cm^{-1} feature is also produced by the D1-D61A (*63, 65*), D1-N181 (*84*), D1-Q165E (*83*), D1-R334A (*83*), and D2-K317A (*81*) mutations. This feature corresponds to a $\nu_{asym}(COO^-)$ mode because it shifts in globally ^{13}C-labeled samples (*101, 102, 106, 117*) but not in globally ^{15}N-labeled samples (*81, 101, 102, 106, 118*). The substantial decrease of the 1544(-) cm^{-1} feature is also produced by the D1-D61A (*63, 65*), D1-E65A (*63*), D1-R334A (*83*), and D2-E312A (*63*) mutations, and to a lesser extent by the D1-E329Q mutation (*63*). The elimination of the 1531(+)/1523(-) cm^{-1} feature is also produced by the D1-D61A (*63, 65*), D1-R334A (*83*), D2-E312 (*63*), and D2-K317A (*81*) mutations and to a lesser extent in some preparations having Sr^{2+} substituted for Ca^{2+} (*94, 113, 115*). The 1544(-) and 1531(+)/1523(-) cm^{-1} features correspond to amide II modes because they shift in both ^{13}C labeled (*101, 102, 106, 117*) and ^{15}N labeled (*81, 101, 102, 106, 118*) samples.

These similarities of the D1-V185N-induced changes in the S_2-S_1 spectrum to those produced by the other mutations imply that the D1-V185N mutation perturbs the same extensive network of hydrogen bonds that is perturbed by the other mutations, as expected from the recent X-ray crystallographic structures (*8-10*). However, the overall extents of the changes to the $\nu_{sym}(COO^-)$ and $\nu_{asym}(COO^-)$/amide II regions are greater than those that are caused by the other mutations, implying that the D1-V185N mutation perturbs the networks of hydrogen bonds

located between Y_Z, D1-D61, and the D1-E65/D1-R334/D2-E312 triad to a greater extent than the other mutations.

In addition to altering features throughout the $\nu_{sym}(COO^-)$ and $\nu_{asym}(COO^-)$/amide II regions of the S_2-S_1 spectrum, the D1-V185N mutation also alters features throughout the S_3-S_2 spectrum. In wild-type PSII, the features in the S_0-S_3 and S_1-S_0 spectra reverse those in the S_2-S_1 and S_3-S_2 spectra (*74-76, 78-80*). Because of the alterations produced by the D1-V185N mutation to the S_2-S_1 and S_3-S_2 spectra, it is not surprising that the mutation produces substantial changes in these regions of the S_0-S_3 and S_1-S_0 spectra. The lower amplitudes of these spectra and the relative absence of features in the S_1-S_0 spectrum may reflect the lower efficiency of the S state transitions in the D1-V185N mutant (*66*).

Networks of H-bonds. The extensive networks of hydrogen bonds in the vicinity of the Mn_4CaO_5 cluster have been studied on the basis of changes to the ν(C=O) modes of protonated carboxylatic acid groups (*63, 65, 81-85*). In the S_2-S_1 spectrum of wild-type, the 1746(-) cm^{-1} feature has been assigned to a carboxylate group whose pK_a value decreases in response to the charge that develops on the Mn_4CaO_5 cluster during the S_1 to S_2 transition. This feature is diminished or eliminated by the D1-D61A, D1-E65A, D1-E329Q, D1-R334A, and D2-E312A mutations, and by overly dehydrating samples (*63, 65, 83*). That the same ν(C=O) mode is altered by all of these mutations and treatments implies the existence of an extensive network of hydrogen bonds that extends at least 20 Å across the Mn_4CaO_5 cluster (*63, 65, 79, 83*). In the S_3-S_2 spectrum of wild-type, the small 1745(+) cm^{-1} feature has been assigned to a carboxylate group whose pK_a value increases in response to the structural changes that occur during the S_2 to S_3 transition. This feature is altered by the D1-D61A mutation and eliminated by the D1-Q165E and D1-E329Q mutations. That the same ν(C=O) mode is altered by all three mutations implies

the existence of an additional network of hydrogen bonds that extends at least 13 Å across the Mn_4CaO_5 cluster (*65, 79, 83*). Elements of these networks of hydrogen bonds may exist only transiently (*58, 119*). During the S_3 to S_0 transition, the 1746(-) cm^{-1} and 1745(+) cm^{-1} features appear to be reversed, resulting in a positive feature at 1746 cm^{-1} in the S_0-S_3 spectrum (*79, 83*). The D1-V185N mutation alters the 1746(-) cm^{-1} feature in the S_2-S_1 spectrum, resulting in a feature with a maximum at 1737 cm^{-1} and a lower frequency shoulder. The mutation also alters the 1745(+) cm^{-1} feature in the S_3-S_2 spectrum, diminishing its intensity and shifting it to 1750 cm^{-1}. These alterations, in particular the 5-9 cm^{-1} shifts, have been observed in no other mutant. The shifts imply that the D1-V185N mutation alters the environments of the carboxylate groups whose pK_a values change in response to the S_1 to S_2 and S_2 to S_3 transitions.

Hydrogen-bonded Water Molecules. The broad positive feature observed between 3200 and 2500 cm^{-1} in the S_2-S_1 spectrum has been studied with QM/MM methods and attributed to the coupled O-H stretching vibrations of strongly hydrogen-bonded water molecules in the network that links D1-D61 with the Ca^{2+} ion and Y_Z (*93*). In the QM/MM analyses, the broad feature is dominated by the O-H stretching vibrations of W1 and W2 (*93*). This feature is eliminated by the D1-D61A mutation (*65*), consistent with the hydrogen bond that exists between this residue and W1 in the recent X-ray crystallographic structural models (*8-10*). The broad positive features in the other S_{n+1}-S_n spectra have been assigned to the strongly hydrogen bonded O-H stretching vibrations of water molecules in networks of hydrogen bonds that are highly polarizable (*88, 95*). That the D1-V185N mutation only slightly perturbed these regions of the S_{n+1}-S_n spectra implies that D1-V185 has limited influence on the networks of hydrogen bonds in the vicinity of W1 and W2.

The features observed between 3700 and 3500 cm^{-1} in the S_2-S_1 spectrum also have been

studied with QM/MM methods. They have been attributed to the coupled O-H stretching vibrations of weakly hydrogen-bonded water molecules in the extended network of hydrogen bonds that links D1-D61 with the Ca^{2+} ion and Y_Z (*93*). The broad negative features observed in the other S_{n+1}-S_n spectra in this region are presumed to have the same origin (*88, 89*). Consequently, these features contain contributions from multiple water molecules. The 3663(-) cm^{-1} and 3617(+) cm^{-1} features in the S_2-S_1 spectrum are diminished by the D1-N181A mutation and eliminated by the D1-D61A and D1-E333Q mutations (*65, 84, 92*). The 3617(+) cm^{-1} feature is also eliminated by the D1-N87A and D1-N87D mutations (*85*). These features are also diminished sharply by the substitution of Sr^{2+} for Ca^{2+} (*94*). The broad negative feature centered at 3603 cm^{-1} in the S_3-S_2 spectrum is also altered by the D1-D61A mutation. Consequently, the Ca^{2+} ion and the D1-D61, D1-N87, D1-N181, and D1-E333 residues all influence the network of hydrogen bonds that links D1-D61 with the Ca^{2+} ion and Y_Z. In the S_2-S_1 spectrum of D1-V185N PSII core complexes, the decrease of the 3663(-) cm^{-1} feature and the replacement of the broad positive 3617 cm^{-1} feature with a broad negative feature centered at 3619 cm^{-1} implies that D1-V185 participates in the same network of hydrogen bonds. The replacement of the 3617(+) cm^{-1} feature with a negative 3619(-) cm^{-1} feature further implies that the perturbation of this extended network by the D1-V185N mutation is at least as substantial as the perturbations introduced by the D1-D61A mutation.

The D-O-D bending region. The H−O−H bending mode [δ(HOH)] is sensitive to hydrogen bond interactions and disappears when a water molecule deprotonates (*96*). Unfortunately, δ(HOH) modes appear near 1640 cm^{-1}, a congested region of the spectrum. In contrast, δ(DOD) modes appear near 1210 cm^{-1}, a region nearly devoid of overlapping protein modes (*96, 105*). Because these modes are very weak, they are detected in $D_2{}^{16}O$-$D_2{}^{18}O$ double

difference spectra (*65, 94, 96*). In such a double difference spectrum, a shift of a single δ(DOD) mode would show as up to four peaks, two from $D_2{}^{16}O$ and two from $D_2{}^{18}O$. Fewer peaks may be observed because of spectral overlap. In wild-type samples, the number of features in the $D_2{}^{16}O$-$D_2{}^{18}O$ double difference spectrum of the S_1 to S_2 transition (Figure 9, upper pair of traces) implies that at least two δ(DOD) modes are shifted during this transition (*65, 94, 96*). In wild-type samples, the amplitudes of most of the features oscillate during the S state cycle. For example, the 1210(+) cm^{-1} feature in the S_2-S_1 double difference spectrum becomes negative (at 1211-1213 cm^{-1}) in the S_3-S_2 and S_0-S_3 double difference spectra and positive again (at 1213 cm^{-1}) in the S_1-S_0 double difference spectrum. Also, the 1221(-) cm^{-1} feature in the S_2-S_1 double difference spectrum becomes positive (at 1225 cm^{-1}) in the S_3-S_2 double difference spectrum and positive (at 1221 cm^{-1}) in the S_0-S_3 double difference spectrum. The oscillations imply that the δ(DOD) modes that are altered during the S_1 to S_2 transition are altered reversibly during the S state cycle (*65, 94, 96*). One of these DOD molecules must form a hydrogen bond with D1-D61 because the D1-D61A mutation eliminates the intense 1221(–) cm^{-1} and 1210(+) cm^{-1} features from the S_2-S_1 $D_2{}^{16}O$-*minus*-$D_2{}^{18}O$ double difference spectrum (*65*). Because the D1-V185N mutation shifted the 1221(-) and 1210(+) cm^{-1} features in this spectrum (and the corresponding 1225(+) and 1213(-) features in the S_3-S_2 double difference spectrum) by only 2-3 cm^{-1} [no more than is observed between different wild-type sample preparations (*65, 94, 96*)], we conclude that the mutation has limited influence on the water molecules that interact with D1-D61. The same conclusion was reached on the basis of the limited perturbations caused by the D1-V185N mutation in the 3200 – 2500 cm^{-1} region of the S_2-S_1 spectrum (see above).

The larger 8-10 cm^{-1} mutation-induced shifts of the 1188(-) and 1174(+) cm^{-1} features in the S_2-S_1 double difference spectrum, in addition to other changes observed between 1200 and

1140 cm^{-1} in the S_2-S_1 and S_3-S_2 double difference spectra, shows that the D1-V185N mutation perturbs at least one water molecule whose bending mode changes reversibly during the S state cycle. This conclusion is consistent with the changes observed between 3700 and 3500 cm^{-1} in the S_2-S_1 spectrum that were attributed to D1-V185N-induced alterations in the extended network of hydrogen bonds that links D1-D61 with the Ca^{2+} ion and Y_Z (see above).

Another D1-V185N-induced alteration to the S_3-S_2 double difference spectrum (Figure 9, second pair of traces) is the decreased intensity of the 1238(-) cm^{-1} feature and its 6 cm^{-1} shift to 1232 cm^{-1}. In wild-type PSII, the 1238(–) cm^{-1} feature in the S_3-S_2 double difference spectra has no positive counterpart in any of the other double difference spectra, implying that the bending mode of one water molecule is eliminated during the S_2 to S_3 transition (*65, 94, 96*). Therefore, the 1238(–) cm^{-1} feature must correspond to a water molecule that deprotonates during the S_2 to S_3 transition (or to a water molecule that physically replaces the water molecule that deprotonates, see below). The 1238(–) cm^{-1} feature in the S_3-S_2 double difference spectrum is eliminated or shifted substantially by the substitution of Sr^{2+} for Ca^{2+} (*94*). Because crystallographic (*120*) and computational (*45, 121, 122*) studies show that the substitution of Sr^{2+} for Ca^{2+} perturbs only W3, W4, and W5, it has been proposed that (1) W3 is the water molecule that deprotonates and joins O5 between Mn4 and Mn1 during the S_2 to S_3 transition and (2) W5 moves to the coordination position on Ca^{2+} vacated by W3 (*94*). Equating W5 with the 1238(–) cm^{-1} feature (*94*) would be consistent with this feature's alteration by the D1-V185N mutation: W5 is within 4.7 Å of D1-V185 in the recent X-ray crystallographic structures of PSII (*8-10*). Consequently, the D1-V185N-induced shift of the 1238(–) cm^{-1} feature in the S_3-S_2 double difference spectrum would be consistent with identifying W3 as the water molecule that deprotonates and joins O5 during the S_2 to S_3 transition.

SUMMARY AND CONCLUSIONS

The D1-V185N mutation perturbs the extensive network of hydrogen bonds that extends from Y_Z to D1-D61 to a greater extent than any other mutation yet examined, yet does not alter water molecules that interact directly with D1-D61. These perturbations are likely the reason that the mutation dramatically slows the structural rearrangement or proton release event that is the rate-limiting step for the S_3 to S_4 transition. The mutation also alters the environments of the carboxylate groups whose pK_a values change in response to the S_1 to S_2 and S_2 to S_3 transitions. Finally, the mutation alters the environment of the water molecule whose bending mode disappears during the S_2 to S_3 transition, consistent with assigning the Ca^{2+}-bound W3 as the water molecule that deprotonates and joins O5 during the S_2 to S_3 transition, possibly as the second substrate water molecule for O_2 formation.

ACKNOWLEDGEMENTS

The authors are grateful to Anh P. Nguyen for maintaining the mutant and wild-type cultures of *Synechocystis* sp. PCC 6803 and for purifying the thylakoid membranes that were used for the isolation of PSII core complexes and to V. S. Batista and coworkers for providing the QM/MM-optimized coordinates for the Mn_4CaO_5 cluster and its environments.

AUTHOR INFORMATION

Corresponding Author

*Email: richard.debus@ucr.edu, Tel.: +1 (951) 827-3483. Fax.: +1 (951) 827-4294. Department of Biochemistry, University of California, Riverside, CA 92521-0129 USA

ORCID

Richard J. Debus: 0000-0003-1321-8730

Present Addresses

⊥ MSU-DOE Plant Research Laboratory, Michigan State University, East Lansing, MI 48824

Funding Sources

Work supported by the Department of Energy, Office of Basic Energy Sciences, Division of Chemical Sciences (grant DE-SC0005291 to R. J. D. for FTIR studies) and by the National Science Foundation (MCB-1716408 to R. L. B. for mutant construction).

Notes

The authors declare no competing financial interests.

ACKNOWLEDGMENT

The authors are grateful to Anh P. Nguyen for maintaining the mutant and wild-type cultures of *Synechocystis* sp. PCC 6803 and for purifying the thylakoid membranes that were used for the isolation of PSII core complexes and to V. S. Batista and coworkers for providing the QM/MM-optimized coordinates for the Mn_4CaO_5 cluster and its environments.

ABBREVIATIONS

Chl, chlorophyll; EDTA, ethylenediaminetetraacetic acid; FTIR, Fourier transform infrared; MES, 2-(N-morpholino)-ethanesulfonic acid; P_{680}, chlorophyll multimer that serves as the light-

induced electron donor in PSII; PSII, photosystem II; Q_A, primary plastoquinone electron acceptor; XFEL, X-ray free electron laser; Y_Z, tyrosine residue that mediates electron transfer between the Mn_4O_5Ca cluster and $P_{680}^{+\bullet}$.

REFERENCES

(1) Cox, N. and Messinger, J. (2013) Reflections on substrate water and dioxygen formation, *Biochim. Biophys. Acta 1827*, 1020-1030.

(2) Yano, J. and Yachandra, V. K. (2014) Mn_4Ca Cluster in Photosynthesis: Where and How Water is Oxidized to Dioxygen, *Chem. Rev. 114*, 4175-4250.

(3) Shen, J.-R. (2015) The Structure of Photosystem II and the Mechanism of Water Oxidation in Photosynthesis, *Annu. Rev. Plant Biol. 66*, 23-48.

(4) Krewald, V., Retegan, M., and Pantazis, D. A. (2016) Principles of Natural Photosynthesis, *Top. Curr. Chem. 371*, 23-48.

(5) Pérez-Navarro, M., Neese, F., Lubitz, W., Pantazis, D. A., and Cox, N. (2016) Recent developments in biological water oxidation, *Curr. Opin. Chem. Biol. 31*, 113-119.

(6) Askerka, M., Brudvig, G. W., and Batista, V. S. (2017) The O_2-Evolving Complex of Photosystem II: Recent Insights from Quantum Mechanics/Molecular Mechanics (QM/MM), Extended X-ray Absorption Fine Structure (EXAFS), and Femtosecond X-ray Crystallography Data, *Acc. Chem. Res. 50*, 41-48.

(7) Vinyard, D. J. and Brudvig, G. W. (2017) Progress Toward a Molecular Mechanism of Water Oxidation in Photosystem II, *Annu. Rev. Phys. Chem. 68*, 101-116.

(8) Umena, Y., Kawakami, K., Shen, J.-R., and Kamiya, N. (2011) Crystal Structure of Oxygen-Evolving Photosystem II at a Resolution of 1.9 Å, *Nature 473*, 55-60.

(9) Suga, M., Akita, F., Hirata, K., Ueno, G., Murakami, H., Nakajima, Y., Shimizu, T., Yamashita, K., Yamamoto, M., Ago, H., and Shen, J.-R. (2015) Native structure of photosystem II at 1.95 Å resolution viewed by femtosecond X-ray pulses, *Nature 517*, 99-103.

(10) Tanaka, A., Fukushi, Y., and Kamiya, N. (2017) Two Different Structures of the Oxygen-Evolving Complex in the Same Polypeptide Frameworks of Photosystem II, *J. Am. Chem. Soc. 139*, 1718-1721.

(11) Ago, H., Adachi, H., Umena, Y., Tashiro, T., Kawakami, K., Kamiya, N., Tian, L., Han, G., Kuang, T., Liu, Z., Wang, F., Zou, H., Enami, I., Miyano, M., and Shen, J.-R. (2016) Novel Features of Eukaryotic Photosystem II Revealed by Its Crystal Structure Analysis from a Red Alga, *J. Biol. Chem. 291*, 5676-5687.

(12) Su, X., Ma, J., Wei, X., Cao, P., Zhu, D., Chang, W., Liu, Z., and Li, M. (2017) Structure and assembly mechanism of plant $C_2S_3M_2$-type PSII-LHCII supercomplex, *Science 357*, 815-820.

(13) Cao, P., Su, X., Pan, X., Liu, Z., Chang, W., and Li, M. (2018) Structure, assembly and energy transfer of plant photosystem II supercomplex, *Biochim. Biophys. Acta* -(in press).

(14) Wei, X., Su, X., Cao, P., Liu, X., Chang, W., Li, M., Zhang, X., and Liu, Z. (2016) Structure of spinach photosystem II-LHII supercomplex at 3.2 A resolution, *Nature 534*, 69-74.

(15) van Bezouwen, L. S., Caffarri, S., Kale, R. S., Kouril, R., Thunnissen, A.-M. W. H., Oostergetal, G. T., and Boekem, E. J. (2017) Subunit and chlorophyll organization of the plant photosystem II supercomplex, *Nature Plants 3*, 17080.

(16) Rapatskiy, L., Cox, N., Savitsky, A., Ames, W. M., Sander, J., Nowaczyk, M. M., Rögner, M., Boussac, A., Neese, F., Messinger, J., and Lubitz, W. (2012) Detection of Water-

Binding Sites of the Oxygen-Evolving Complex of Photosystem II Using W-band ^{17}O Electron-Electron Double Resonance-Detected NMR Spectroscopy, *J. Am. Chem. Soc. 134*, 16619-16634.

(17) Pérez Navarro, M., Ames, W. M., Nilsson, H., Lohmiller, T., Pantazis, D. A., Rapatskiy, L., Nowaczyk, M. M., Neese, F., Boussac, A., Messinger, J., Lubitz, W., and Cox, N. (2013) Ammonia binding to the oxygen-evolving complex of photosystem II identified the solvent-exchangeable oxygen bridge (μ-oxo) of the manganese tetramer, *Proc. Natl. Acad. Sci. USA 110*, 15561-15566.

(18) Lohmiller, T., Krewald, V., Pérez Navarro, M., Retegan, M., Rapatskiy, L., Nowaczyk, M. M., Boussac, A., Neese, F., Lubitz, W., Pantazis, D. A., and Cox, N. (2014) Structure, ligands and substrate coordination of the oxygen-evolving complex of photosystem II in the S_2 state: a combined EPR and DFT study, *Phys. Chem. Chem. Phys. 16*, 11877-11892.

(19) Lohmiller, T., Krewald, V., Sedoud, A., Rutherford, A. W., Neese, F., Lubitz, W., Pantazis, D. A., and Cox, N. (2017) The First State in the Catalytic Cycle of the Water-Oxidizing Enzyme: Identification of a Water-Derived μ-Hydroxo Bridge, *J. Am. Chem. Soc. 139*, 14412-14424.

(20) Pantazis, D. A., Ames, W., Cox, N., Lubitz, W., and Neese, F. (2012) Two Interconvertable Structures that Explain the Spectroscopic Properties of the Oxygen-Evolving Complex of Photosystem II in the S_2 State, *Angew. Chem. Int. Ed. 51*, 9935-9940.

(21) Siegbahn, P. E. M. (2008) A Structure-Consistent Mechanism for Dioxygen Formation in Photosystem II, *Chem. Eur. J. 14*, 8290-8302.

(22) Siegbahn, P. E. M. (2013) Water oxidation mechanism in photosystem II, including oxidations, proton release pathways, O-O bond formation and O_2 release, *Biochim. Biophys. Acta 1827*, 1003-1019.

(23) Cox, N., Retegan, M., Neese, F., Pantazis, D. A., Boussac, A., and Lubitz, W. (2014) Electronic structure of the oxygen-evolving complex in photosystem II prior to O-O bond formation, *Science 345*, 804-808.

(24) Zaharieva, I., Chernev, P., Berggren, G., Anderlund, M., Styring, S., Dau, H., and Haumann, M. (2016) Room-Temperature Energy-Sampling Kβ X-ray Emission Spectroscopy of the Mn_4Ca Complex of Photosystem II Reveals Three Manganese-Centered Oxidation Steps and Suggests Coordination Change Prior to O_2 Formation, *Biochemistry 55*, 4197-4211.

(25) Suga, M., Akita, F., Sugahara, M., Kubo, M., Nakajima, Y., Nakane, T., Yamashita, K., Umena, Y., Nakabayashi, M., Yamane, T., Nakano, T., Suzuki, M., Masuda, T., Inoue, S., Kimura, T., Nomura, T., Yonekura, S., Yu, L.-J., Sakamoto, T., Motomura, T., Chen, J.-H., Kato, Y., Noguchi, T., Tono, K., Joti, Y., Kameshima, T., Hatsui, T., Nango, E., Tanaka, R., Naitow, H., Matsuura, Y., Yamashita, A., Yamamoto, M., Nureki, O., Yabashi, M., Ishikawa, T., Iwata, S., and Shen, J.-R. (2017) LIght-induced structural changes and the site of O=O bond formation in PSII caught by XFEL, *Nature 543*, 131-135.

(26) Askerka, M., Vinyard, D. J., Brudvig, G. W., and Batista, V. S. (2015) NH_3 Binding to the S_2 State of the O_2-Evolving Complex of Photosystem II: Analogue to H_2O Binding during the S_2 to S_3 Transition, *Biochemistry 54*, 5783-5786.

(27) Capone, M., Bovi, D., Narzi, D., and Guidoni, L. (2016) Reorganization of Substrate Waters between the Closed and Open Cubane Conformers during the S_2 to S_3 Transition in the Oxygen Evolving Complex, *Biochemistry 54*, 6439-6442.

(28) Askerka, M., Wang, J., Vinyard, D. J., Brudvig, G. W., and Batista, V. S. (2016) S_3 State of the O2-Evolving Complex of Photosystem II: Insights from QM/MM, EXAFS, and Femtosecond X-ray Diffraction, *Biochemistry 55*, 984.

(29) Retegan, M., Krewald, V., Mamedov, F., Neese, F., Lubitz, W., Cox, N., and Pantazis, D. A. (2016) A five-coordinate Mn(IV) intermediate in biological water oxidation: spectroscopic signature and a pivot mechanism for water binding, *Chem. Sci. 7*, 72-84.

(30) Capone, M., Narzi, D., Bovi, D., and Guidoni, L. (2016) Mechanism of Water Delivery to the Active Site of Photosystem II along the S_2 to S_3 Transition, *J. Phys. Chem. Lett. 7*, 592-596.

(31) Retegan, M. and Pantazis, D. A. (2016) Interaction of methanol with the oxygen-evolving complex: atomistic models, channel identification, species dependence, and mechanistic implications, *Chem. Sci. 7*, 6463-6476.

(32) Wang, J., Askerka, M., Brudvig, G. W., and Batista, V. S. (2017) Crystallographic Data Support the Carousel Mechanism of Water Supply to the Oxygen-Evolving Complex of Photosystem II, *ACS Energy Lett. 2*, 2299-2306.

(33) Ames, W., Pantazis, D. A., Krewald, V., Cox, N., Messinger, J., Lubitz, W., and Neese, F. (2011) Theoretical Evaluation of Structural Models of the S_2 State in the Oxygen Evolving Complex of Photosystem II: Protonation States and Magnetic Interactions, *J. Am. Chem. Soc. 133*, 19743-19757.

(34) Bovi, D., Narzi, D., and Guidoni, L. (2013) The S_2 State of the Oxygen-Evolving Complex of Photosystem II Explored by QM/MM Dynamics: Spin Surfaces and Metastable States Suggest a Reaction Path Towards the S_3 State, *Angew. Chem. Int. Ed. 52*, 11744-11749.

(35) Shoji, M., Isobe, H., and Yamaguchi, K. (2015) QM/MM study of the S_2 to S_3 transition reaction in the oxygen-evolving complex of photosystem II, *Chem. Phys. Lett. 636*, 172-179.

(36) Isobe, H., Shoji, M., Shen, J.-R., and Yamaguchi, K. (2015) Strong Coupling between the Hydrogen Bonding Environment and Redox Chemistry during the S_2 to S_3 Transition in the Oxygen-Evolving Complex of Photosystem II, *J. Phys. Chem. B 119*, 13922-13933.

(37) Ugur, I., Rutherford, A. W., and Kaila, V. R. I. (2016) Redox-coupled substrate water reorganization in the active site of Photosystem II - The role of calcium in substrate water delivery, *Biochim. Biophys. Acta 1857*, 740-748.

(38) Beal, N. J., Corry, T. A., and O'Malley, P. J. (2018) A Comparison of Experimental and Broken Symmetry Density Functional (BS-DFT) Calculated Electron Paramagnectic Resonance (EPR) Parameters for Intermediates Involved in the S_2 to S_3 State Transition of Nature's Oxygen Evolving Complex, *J. Phys. Chem. B 122*, 1394-1407.

(39) Siegbahn, P. E. M. (2009) Structures and Energetics for O_2 Formation in Photosystem II, *Acc. Chem. Res. 42*, 1871-1880.

(40) Li, X. and Siegbahn, P. E. M. (2015) Alternative mechanisms for O_2 release and O-O bond formation in the oxygen evolving complex of photosystem II, *Phys. Chem. Chem. Phys. 17*, 12168-12174.

(41) Krewald, V., Retegan, M., Neese, F., Lubitz, W., Pantazis, D. A., and Cox, N. (2016) Spin State as a Marker for the Structural Evolution of Nature's Water-Splitting Catalyst, *Inorg. Chem. 55*, 488-501.

(42) Siegbahn, P. E. M. (2018) Water Oxidation by PSII: A Quantum Chemical Approach, in *Mechanisms of Primary Energy Transduction in Biology* (Wikström, M., Ed.) pp 273-295, Royal Society of Chemistry, London.

(43) Siegbahn, P. E. M. (2006) O-O Bond Formation in the S_4 State of the Oxygen-Evolving Complex in Photosystem II, *Chem. Eur. J. 12*, 9217-9227.

(44) Nilsson, H., Rappaport, F., Boussac, A., and Messinger, J. (2014) Substrate-water exchange in photosystem II is arrested before dioxygen formation, *Nature Commun. 5*, 4305-doi:10.1038/ncomms5305.

(45) Vogt, L., Ertem, M. Z., Pal, R., Brudvig, G. W., and Batista, V. S. (2015) Computational Insights on Crystal Structures of the Oxygen-Evolving Complex of Photosystem II with Either Ca^{2+} or Ca^{2+} Substituted by Sr^{2+}, *Biochemistry 54*, 820-825.

(46) Klauss, A., Haumann, M., and Dau, H. (2012) Alternating electron and proton transfer steps in photosynthetic water oxidation, *Proc. Natl. Acad. Sci. USA 109*, 16035-16040.

(47) Klauss, A., Haumann, M., and Dau, H. (2015) Seven Steps of Alternating Electron and Proton Transfer in Photosystem II Water Oxidation Traced by Time-Resolved Photothermal Beam Deflection at Improved Sensitivity, *J. Phys. Chem. B 119*, 2677-2689.

(48) Zaharieva, I., Dau, H., and Haumann, M. (2017) Sequential and Coupled Proton and Electron Transfer Events in the S_2 to S_3 Transition of Photosynthetic Water Oxidation Revealed by Time-Resolved X-ray Absorption Spectroscopy, *Biochemistry 55*, 6996-7004.

(49) Murray, J. W. and Barber, J. (2007) Structural Characteristics of Channels and Pathways in Photosystem II Including the Identification of an Oxygen Channel, *J. Struct. Biol. 159*, 228-237.

(50) Gabdulkhakov, A., Guskov, A., Broser, M., Kern, J., Müh, F., Saenger, W., and Zouni, A. (2009) Probing the Accessibility of the Mn_4Ca Cluster in Photosystem II: Channels Calculation, Noble Gas Derivatization, and Cocrystallization with DMSO, *Structure 17*, 1223-1234.

(51) Bondar, A.-N. and Dau, H. (2012) Extended protein/water H-bond networks in photosynthetic water oxidation, *Biochim. Biophys. Acta 1817*, 1177-1190.

(52) Vassiliev, S., Zaraiskaya, T., and Bruce, D. (2012) Exploring the energetics of water permeation in photosystem II by multiple steered molecular dynamics simulations, *Biochim. Biophys. Acta 1817*, 1671-1678.

(53) Ogata, K., Yuki, T., Hatakeyama, M., Uchida, W., and Nakamura, S. (2013) All-Atom Molecular Dynamics Simulation of Photosystem II Embedded in Thylakoid Membranes, *J. Am. Chem. Soc. 135*, 15670-15673.

(54) Bao, H., Dilbeck, D. L., and Burnap, R. L. (2013) Proton transport facilitating water-oxidation: the role of second sphere ligands surrounding the catalytic metal cluster, *Photosynth. Res. 116*, 215-219.

(55) Linke, K. and Ho, F. M. (2014) Water in Photosystem II: Structural, functional, and mechanistic considerations, *Biochim. Biophys. Acta 1837*, 14-32.

(56) Vogt, L., Vinyard, D. J., Khan, S., and Brudvig, G. W. (2015) Oxygen-evolving complex of Photosystem II: an analysis of second-shell residues and hydrogen-bonding networks, *Curr. Opin. Chem. Biol. 25*, 152-158.

(57) Takoaka, T., Sakashita, N., Saito, K., and Ishikita, H. (2016) pK_a of a Proton-Conducting Water Chain in Photosystem II, *J. Phys. Chem. Lett. 7*, 1925-1932.

(58) Guerra, F., Siemers, M., Mielack, C., and Bondar, A.-N. (2018) Dynamics of Long-Distance Hydrogen-Bond Networks in Photosystem II, *J. Phys. Chem. B* 4625-4641.

(59) Hundelt, M., Hays, A.-M. A., Debus, R. J., and Junge, W. (1998) Oxygenic Photosystem II: The Mutation D1-D61N in *Synechocystis* sp. PCC 6803 Retards S-State

Transitions without Affecting Electron Transfer from Y_Z to P_{680}^+, *Biochemistry 37*, 14450-14456.

(60) Clausen, J., Debus, R. J., and Junge, W. (2004) Time-Resolved Oxygen Production by PSII: Chasing Chemical Intermediates, *Biochim. Biophys. Acta 1655*, 184-194.

(61) Ferreira, K. N., Iverson, T. M., Maghlaoui, K., Barber, J., and Iwata, S. (2004) Architecture of the Photosynthetic Oxygen-Evolving Center, *Science 303*, 1831-1838.

(62) Ishikita, H., Saenger, W., Loll, B., Biesiadka, J., and Knapp, E.-W. (2006) Energetics of a Possible Proton Exit Pathway for Water Oxidation in Photosystem II, *Biochemistry 45*, 2063-2071.

(63) Service, R. J., Hillier, W., and Debus, R. J. (2010) Evidence from FTIR Difference Spectroscopy of an Extensive Network of Hydrogen Bonds near the Oxygen-Evolving Mn_4Ca Cluster of Photosystem II Involving D1-Glu65, D2-Glu312, and D1-Glu329, *Biochemistry 49*, 6655-6669.

(64) Dilbeck, D. L., Hwang, H. J., Zaharieva, I., Gerencser, L., Dau, H., and Burnap, R. L. (2012) The D1-D61N Mutation in *Synechocystis* sp. PCC 6803 Allows the Observation of pH-Sensitive Intermediates in the Formation and Release of O_2 from Photosystem II, *Biochemistry 51*, 1079-1091.

(65) Debus, R. J. (2014) Evidence from FTIR Difference Spectroscopy That D1-Asp61 Influences the Water Reactions of the Oxygen-Evolving Mn_4CaO_5 Cluster of Photosystem II, *Biochemistry 53*, 2941-2955.

(66) Dilbeck, D. L., Bao, H., Neveu, C. L., and Burnap, R. L. (2013) Perturbing the Water Cavity Surrounding the Manganese Cluster by Mutating the Residue D1-Valine Has a Strong Effect on the Water Oxidation Mechanism of Photosystem II, *Biochemistry 52*, 6824-6833.

(67) Haumann, M., Liebisch, P., Müller, C., Barra, M., Grabolle, M., and Dau, H. (2005) Photosynthetic O_2 Formation Tracked by Time-Resolved X-ray Experiments, *Science 310*, 1019-1021.

(68) Gerencsér, L. and Dau, H. (2010) Water Oxidation by Photosystem II: H_2O-D_2O Exchange and the Influence of pH Support Formation of an Intermediate by Removal of a Proton before Dioxygen Creation, *Biochemistry 49*, 10098-10106.

(69) Bao, H. and Burnap, R. L. (2015) Structural rearrangements preceding dioxygen formation by the water oxidation complex of photosystem II, *Proc. Natl. Acad. Sci. USA 112*, E6139-E6147.

(70) Zscherp, C. and Barth, A. (2001) Reaction-Induced Infrared Difference Spectroscopy for the Study of Protein Reaction Mechanisms, *Biochemistry 40*, 1875-1883.

(71) Barth, A. and Zscherp, C. (2002) What Vibrations Tell Us About Proteins, *Q. Rev. Biophys. 35*, 369-430.

(72) Rich, P. R. and Iwaki, M. (2005) Infrared Protein Spectroscopy as a Tool to Study Protonation Reactions Within Proteins, in *Biophysical and Structural Aspects of Bioenergetics* (Wikström, M., Ed.) pp 314-333, Royal Society of Chemistry, Cambridge, U.K.

(73) Barth, A. (2007) Infrared Spectroscopy of Proteins, *Biochim. Biophys. Acta 1767*, 1073-1101.

(74) Noguchi, T. (2007) Light-Induced FTIR Difference Spectroscopy as a Powerful Tool Toward Understanding the Molecular Mechanism of Photosynthetic Oxygen Evolution, *Photosyn. Res. 91*, 59-69.

(75) Noguchi, T. (2008) Fourier Transform Infrared Analysis of the Photosynthetic Oxygen-Evolving Center, *Coord. Chem. Rev. 251*, 336-346.

(76) Debus, R. J. (2008) Protein Ligation of the Photosynthetic Oxygen-Evolving Center, *Coord. Chem. Rev. 252*, 244-258.

(77) Chu, H.-A. (2013) Fourier transform infrared difference spectroscopy for studying the molecular mechanism of photosynthetic water oxidation, *Frontiers Plant Sci. 4*, 146.

(78) Noguchi, T. (2013) Monitoring the reactions of photosynthetic water oxidation using infrared spectroscopy, *Biomedical Spectroscopy and Imaging 2*, 115-128.

(79) Debus, R. J. (2015) FTIR Studies of Metal Ligands, Networks of Hydrogen Bonds, and Water Molecules near the Active Site Mn_4CaO_5 Cluster in Photosystem II, *Biochim. Biophys. Acta 1847*, 19-34.

(80) Noguchi, T. (2015) Fourier transform infrared difference and time-resolved infrared detection of the electron and proton transfer dynamics in photosynthetic water oxidation, *Biochim. Biophys. Acta 1847*, 35-45.

(81) Pokhrel, R., Service, R. J., Debus, R. J., and Brudvig, G. W. (2013) Mutation of Lysine 317 in the D2 Subunit of Photosystem II Alters Chloride Binding and Proton Transport, *Biochemistry 52*, 4758-4773.

(82) Suzuki, H., Yu, J., Kobayashi, T., Nakanishi, H., Nixon, P. J., and Noguchi, T. (2013) Functional Roles of D2-Lys317 and the Interacting Chloride Ion in the Water Oxidation Reaction of Photosystem II As Revealed by Fourier Transform Infrared Analysis, *Biochemistry 52*, 4748-4757.

(83) Service, R. J., Hillier, W., and Debus, R. J. (2014) A Network of Hydrogen Bonds near the Oxygen-Evolving Mn_4CaO_5 Cluster of Photosystem II Probed with FTIR Difference Spectroscopy, *Biochemistry 53*, 1001-1017.

(84) Pokhrel, R., Debus, R. J., and Brudvig, G. W. (2015) Probing the Effect of Mutations of Asparagine 181 in the D1 Subunit of Photosystem II, *Biochemistry 54*, 1663-1672.

(85) Banerjee, G., Ghosh, I., Kim, C. J., Debus, R. J., and Brudvig, G. W. (2017) Substitution of the D1-N87 site in photosystem II of cyanobacteria mimics the chloride-binding characteristics of spinach photosystem II, *J. Biol. Chem. 293*, 2487-2497.

(86) Nakamura, S. and Noguchi, T. (2017) Infrared Determination of the Protonation State of a Key Histidine Residue in the Photosynthetic Water Oxidizing Center, *J. Am. Chem. Soc. 139*, 9364-9375.

(87) Noguchi, T. and Sugiura, M. (2000) Structure of an Active Water Molecule in the Water-Oxidizing Complex of Photosystem II as Studied by FTIR Spectroscopy, *Biochemistry 39*, 10943-10949.

(88) Noguchi, T. and Sugiura, M. (2002) FTIR Detection of Water Reactions During the Flash-Induced S-State Cycle of the Photosynthetic Water-Oxidizing Complex, *Biochemistry 41*, 15706-15712.

(89) Noguchi, T. (2007) FTIR Detection of Water Reactions in the Oxygen-Evolving Center of Photosystem II, *Phil. Trans. R. Soc. Lond. B 363*, 1189-1195.

(90) Shimada, Y., Suzuki, H., Tsuchiya, T., Tomo, T., Noguchi, T., and Mimuro, M. (2009) Effect of a Single-Amino Acid Substitution of the 43 kDa Chlorophyll Protein on the Oxygen-Evolving Reaction of the Cyanobacterium *Synechocystis* sp. PCC 6803: Analysis of the Glu354Gln Mutation., *Biochemistry 48*, 6095-6103.

(91) Hou, L.-H., Wu, C.-M., Huang, H.-H., and Chu, H.-A. (2011) Effects of Ammonia on the Structure of the Oxygen-Evolving Complex in Photosystem II As Revealed by Light-Induced FTIR Difference Spectroscopy, *Biochemistry 50*, 9248-9254.

(92) Service, R. J., Yano, J., Dilbeck, D. L., Burnap, R. L., Hillier, W., and Debus, R. J. (2013) Participation of Glutamate-333 of the D1 Polypeptide in the Ligation of the Mn_4CaO_5 Cluster in Photosystem II, *Biochemistry 52*, 8452-8464.

(93) Nakamura, S., Ota, K., Shibuya, Y., and Noguchi, T. (2016) Role of a Water Network around the Mn_4CaO_5 Cluster in Photosynthetic Water Oxidation: A Fourier Transform Infrared Spectroscopy and Quantum Mechanics/Molecular Mechanics Calculation Study, *Biochemistry 55*, 597-607.

(94) Kim, C. J. and Debus, R. J. (2017) Evidence from FTIR Difference Spectroscopy That a Substrate H_2O Molecule for O_2 Formation in Photosystem II is Provided by the Ca Ion of the Catalytic Mn_4CaO_5 Cluster, *Biochemistry 56*, 2558-2570.

(95) Noguchi, T., Suzuki, H., Tsuno, M., Sugiura, M., and Kato, C. (2012) Time-Resolved Infrared Detection of the Proton and Protein Dynamics during Photosynthetic Oxygen Evolution, *Biochemistry 51*, 3205-3214.

(96) Suzuki, H., Sugiura, M., and Noguchi, T. (2008) Monitoring Water Reactions during the S-State Cycle of the Photosynthetic Water-Oxidizing Center: Detection of the DOD Bending Vibrations by Means of Fourier Transform Infrared Spectroscopy, *Biochemistry 47*, 11024-11030.

(97) Debus, R. J., Campbell, K. A., Gregor, W., Li, Z.-L., Burnap, R. L., and Britt, R. D. (2001) Does Histidine 332 of the D1 Polypeptide Ligate the Manganese Cluster in Photosystem II? An Electron Spin Echo Envelope Modulation Study, *Biochemistry 40*, 3690-3699.

(98) Strickler, M. A., Walker, L. M., Hillier, W., Britt, R. D., and Debus, R. J. (2007) No Evidence from FTIR Difference Spectroscopy That Aspartate-342 of the D1 Polypeptide Ligates

a Mn Ion That Undergoes Oxidation during the S_0 to S_1, S_1 to S_2, or S_2 to S_3 Transitions in Photosystem II, *Biochemistry 46*, 3151-3160.

(99) Hays, A.-M. A., Vassiliev, I. R., Golbeck, J. H., and Debus, R. J. (1998) Role of D1-His190 in Proton-Coupled Electron Transfer Reactions in Photosystem II: A Chemical Complementation Study, *Biochemistry 37*, 11352-11365.

(100) Noguchi, T. and Sugiura, M. (2002) Flash-Induced FTIR Difference Spectra of the Water Oxidizing Complex in Moderately Hydrated Photosystem II Core Films: Effect of Hydration Extent on S-State Transitions, *Biochemistry 41*, 2322-2330.

(101) Noguchi, T. and Sugiura, M. (2003) Analysis of Flash-Induced FTIR Difference Spectra of the S-State Cycle in the Photosynthetic Water-Oxidizing Complex by Uniform ^{15}N and ^{13}C Isotope Labeling, *Biochemistry 42*, 6035-6042.

(102) Yamanari, T., Kimura, Y., Mizusawa, N., Ishii, A., and Ono, T.-A. (2004) Mid- to Low-Frequency Fourier Transform Infrared Spectra of S-State Cycle for Photosynthetic Water Oxidation in *Synechocystis* sp. PCC 6803, *Biochemistry 43*, 7479-7490.

(103) Noguchi, T., Inoue, Y., and Tang, X.-S. (1999) Structure of a Histidine Ligand in the Photosynthetic Oxygen-Evolving Complex as Studied by Light-Induced Fourier Transform Infrared Spectroscopy, *Biochemistry 38*, 10187-10195.

(104) Kandori, H. and Shichida, Y. (2000) Direct Observation of the Bridged Water Stretching Vibrations Inside a Protein, *J. Am. Chem. Soc. 122*, 11745-11746.

(105) Venyaminov, S. Yu. and Prendergast, F. G. (1997) Water (H_2O and D_2O) Molar Aborptivity in the 1000-4000 cm^{-1} Range and Quantitative Infrared Spectroscpy of Aqueous Solutions, *Anal. Biochem. 248*, 234-245.

(106) Kimura, Y., Mizusawa, N., Ishii, A., Yamanari, T., and Ono, T.-A. (2003) Changes of Low-Frequency Vibrational Modes Induced by Universal ^{15}N- and ^{13}C-Isotope Labeling in S_2/S_1 FTIR Difference Spectrum of Oxygen-Evolving Complex, *Biochemistry 42*, 13170-13177.

(107) Nakamura, S. and Noguchi, T. (2016) Quantum mechanics/molecular mechanics simulation of the ligand vibrations of the water-oxidizing Mn_4CaO_5 cluster in photosystem II, *Proc. Natl. Acad. Sci. USA 113*, 12727-12732.

(108) Chu, H.-A., Debus, R. J., and Babcock, G. T. (2001) D1-Asp170 is Structurally Coupled to the Oxygen Evolving Complex in Photosystem II as Revealed by Light-Induced Fourier Transform Infrared Difference Spectroscopy, *Biochemistry 40*, 2312-2316.

(109) Debus, R. J., Strickler, M. A., Walker, L. M., and Hillier, W. (2005) No Evidence from FTIR Difference Spectroscopy That Aspartate-170 of the D1 Polypeptide Ligates a Manganese Ion That Undergoes Oxidation during the S_0 to S_1, S_1 to S_2, or S_2 to S_3 Transitions in Photosystem II, *Biochemistry 44*, 1367-1374.

(110) Kimura, Y., Mizusawa, N., Ishii, A., Nakazawa, S., and Ono, T.-A. (2005) Changes in Structural and Functional Properties of Oxygen-Evolving Complex Induced by Replacement of D1-Glutamate 189 with Glutamine in Photosystem II: Ligation of Glutamate 189 Carboxylate to the Manganese Cluster, *J. Biol. Chem. 280*, 37895-37900.

(111) Strickler, M. A., Hillier, W., and Debus, R. J. (2006) No Evidence from FTIR Difference Spectroscopy that Glutamate-189 of the D1 Polypeptide Ligates a Mn Ion that Undergoes Oxidation During the S_0 to S_1, S_1 to S_2, or S_2 to S_3 Transitions in Photosystem II, *Biochemistry 45*, 8801-8811.

(112) Debus, R. J. (2016) Identifying carboxylate ligand vibrational modes in photosystem II with QM/MM methods, *Proc. Natl. Acad. Sci. USA 113*, 12613-12615.

(113) Strickler, M. A., Walker, L. M., Hillier, W., and Debus, R. J. (2005) Evidence from Biosynthetically Incorporated Strontium and FTIR Difference Spectroscopy that the C-Terminus of the D1 Polypeptide of Photosystem II Does Not Ligate Calcium, *Biochemistry 44*, 8571-8577.

(114) De Riso, A., Jenson, D. L., and Barry, B. A. (2010) Calcium Exchange and Structural Changes during the Photosynthetic Oxygen Evolving Cycle, *Biophys. J. 91*, 1999-2008.

(115) Suzuki, H., Taguchi, Y., Sugiura, M., Boussac, A., and Noguchi, T. (2006) Structural Perturbations of the Carboxylate Ligands to the Mn Cluster upon Ca^{2+}/Sr^{2+} Exchange in the S-state Cycle of Photosynthetic Oxygen Evolution as Studied by Flash-Induced FTIR Difference Spectroscopy, *Biochemistry 45*, 13454-13464.

(116) Polander, B. C. and Barry, B. A. (2013) Calcium, Strontium, and Protein Dynamics during the S_2 to S_3 Transition in the Photosynthetic Oxygen-Evolving Cycle, *J. Phys. Chem. Lett. 4*, 3356-3362.

(117) Noguchi, T., Sugiura, M., and Inoue, Y. (1999) FTIR Studies on the Amino-Acid Ligands of the Photosynthetic Oxygen-Evolving Mn-Cluster, in *Fourier Transform Spectroscopy: Twelfth International Conference* (Itoh, K. and Tasumi, M., Eds.) pp 459-460, Waseda University Press, Tokyo, Japan.

(118) Service, R. J., Yano, J., McConnell, I., Hwang, H. J., Niks, D., Hille, R., Wydrzynski, T., Burnap, R. L., Hillier, W., and Debus, R. J. (2011) Participation of Glutamate-354 of the CP43 Polypeptide in the Ligation of Manganese and the Binding of Substrate Water in Photosystem II, *Biochemistry 50*, 63-81.

(119) del Val, C., Bondar, L., and Bondar, A.-N. (2014) Coupling between inter-helical hydrogen bonding and water dynamics in a proton transporter, *J. Struct. Biol. 186*, 95-111.

(120) Koua, F. H. M., Umena, Y., Kawakami, K., and Shen, J.-R. (2013) Structure of Sr-substituted photosystem II at 2.1 Å resolution and its implications in the mechanism of water oxidation, *Proc. Natl. Acad. Sci. USA 110*, 3889-3894.

(121) Terrett, R., Petrie, S., Pace, R. J., and Stranger, R. (2014) What does the Sr-substituted 2.1 Å resolution crystal structure of photosystem II reveal about the water oxidation mechanism?, *Chem. Commun. 50*, 3187-3190.

(122) Pitari, F., Bovi, D., Narzi, D., and Guidoni, L. (2015) Characterization of the Sr^{2+}- and Cd^{2+}-Substituted Oxygen-Evolving Complex of Photosystem II by Quantum Mechanics/Molecular Mechanics Calculations, *Biochemistry 54*, 5959-5968.

For Table of Contents Use Only

Impact of D1-V185 on the Water Molecules that facilitate O_2 Formation by the Catalytic Mn_4CaO_5 Cluster in Photosystem II †

Christopher J. Kim, Han Bao, Robert L. Burnap, and Richard J. Debus *